Impact of generation current on the evaluation of the depletion width in heavily irradiated Si detectors

E. Gaubas,[a] T. Čeponis, and J. Vaitkus
Institute of Applied Research, Vilnius University, 10222 Vilnius, Lithuania

(Received 17 March 2011; accepted 24 June 2011; published online 10 August 2011)

The depletion width and full depletion condition are essential parameters in the search for radiation tolerant detector design and operational regimes. In this work, results of measurements of barrier capacitance by combining a transient technique for barrier evaluation by linearly increasing voltage (BELIV), with temperature dependent capacitance-voltage and current-voltage characteristics of neutron irradiated Si pin detectors are discussed. It is shown that the generation current, caused by a high density of radiation induced traps, distorts the capacitance measurements in heavily irradiated devices. There is no space charge sign inversion effect, however, and heavily irradiated detectors become fully depleted in equilibrium. © *2011 American Institute of Physics*. [doi:10.1063/1.3619802]

I. INTRODUCTION

The anticipated upgrade of the Super-Large Hadron Collider (S-LHC) leads to a need for radiation hard detectors capable to survive hadron fluences up of 10^{16} cm^{-2}.[1] In view of the operational regimes for functioning of the LHC, high resistivity n-Si detectors were designed based on the paradigm[1–4] of sign inversion of the effective doping density caused by interplay of intentionally introduced shallow impurity centers and radiation defects. The effective dopant density is commonly evaluated by routine capacitance-voltage (C-V) measurements and extraction of the full depletion voltage (V_{FD}). The value of V_{FD} is determined either as a saturation point on the C-V characteristic or by the transient current technique (TCT) using a kink-point on the characteristic of voltage dependent variations of the injected charge drift transients.[5] Having determined V_{FD} by the mentioned measurement procedures, the effective doping density N_{eff} is calculated using the relation $N_{eff} \cong 2\varepsilon\varepsilon_0 V_{FD}/ed^2$, valid only for a perfect diode. Here the widely used symbols represent: ε and ε_0 material and vacuum permittivity, e the elementary charge, and d the diode thickness. The reduction of N_{eff} to a minimum value with increasing irradiation fluence has been obtained for high resistivity ($N_D \sim 10^{12}$ cm^{-3}) Si detectors in the range of rather low fluences $\sim 3 \times 10^{12}$ cm^{-2}. It has also been shown[6] that the minimum of the effective doping concentration versus fluence shifts to higher fluences with increased initial doping. Having obtained a minimum of N_{eff} and V_{FD} as a function of fluence, further increase of N_{eff} and V_{FD} with fluence (Φ) was evaluated to values of $N_{eff} > 10^{14}$ cm^{-3}and $V_{FD} > 600$ V.[1,3,4] These values of N_{eff} and V_{FD} determined for 300 μm thick diodes[7] are however doubtful, when the critical width and voltages $U_{r\,cr} \cong 5.3 \times 10^{13} N_{eff}{}^{-3/4}$ (Ref. 8) for avalanche breakdown are significantly exceeded. However, no avalanche breakdown effects were observed. Contrarily, current-voltage (I-V) characteristics show close to symmetric behavior for reverse and forward biasing.

Therefore, in this work a combined analysis of fluence dependent C-V and I-V characteristics and barrier as well as storage capacitance determined transients induced by linearly increasing voltage (LIV) pulses[9] has been performed to clarify the depletion width and full depletion voltage dependence on irradiation fluence. This approach is preferable to having a constant ramp of the external voltage variation and of the electric field induced displacement current. The measurement technique, using LIV pulsed transients, is applied for the characterization of disordered structures.[10]

II. SAMPLES, MEASUREMENT TECHNIQUES AND EXPERIMENTAL RESULTS

A set of magnetic field assisted Czochralski (MCZ) grown, high resistivity Si p^+nn^+ pad-detectors irradiated by reactor neutrons with fluence Φ in the range of $10^{12} - 10^{16}$ cm^{-2} (Ref. 1), has been examined.

The fluence dependent C-V and I-V characteristics, respectively, are illustrated in Fig. 1

The C-V characteristics, measured at room temperature and using both the parallel (C_p) and serial (C_s) circuit regimes and 100 kHz frequency by a QuadTech-7600B LRC-meter, are illustrated in Fig. 1(a). The ac test signal was kept as small as possible, $\leq$20 mV. The parallel (C_p) and serial (C_s) circuit regimes have been used to control the requirement of low parallel conductance and of low series resistance, as discussed in Ref. 11, for correct C measurements. It is clearly observed that the C_p and C_s dependencies on reverse voltage as well as the values of C_p, C_s coincide for samples irradiated with $\Phi \leq 10^{13}$ n/cm^2. Although, the absolute value of C_s decreases with increasing fluence. However, significant differences between C_p and C_s appear in heavier ($\Phi > 10^{13}$ n/cm^2) irradiated diodes. This result is in a quantitative agreement with published data on irradiated Si detectors,[7] taking into account the differences in frequency. The differences between C_p and C_s indicate that the standard

[a]Author to whom correspondence should be addressed. Electronic mail: eugenijus.gaubas@ff.vu.lt.

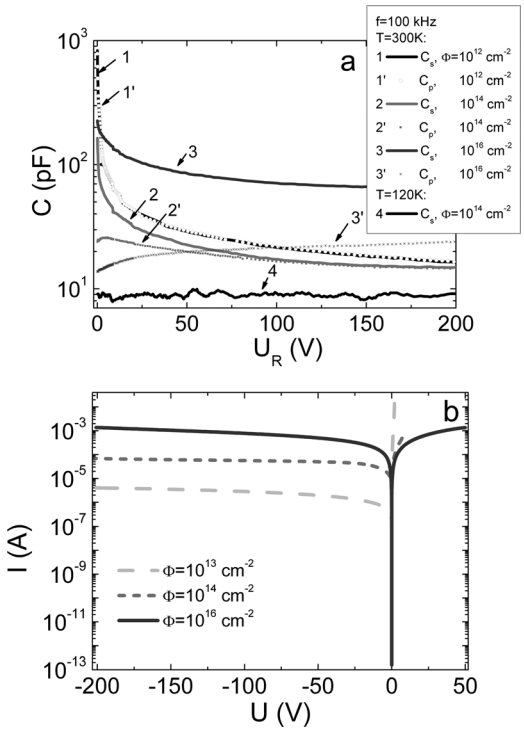

FIG. 1. Fluence dependent variations of capacitance-voltage (a) and current-voltage (b) characteristics.

analysis for the extraction of C values is no longer valid for the diodes irradiated with $\Phi > 10^{13}$ n/cm^2. The main reason is the generation current and a non-linear voltage sharing between circuit elements within the LRC-meter due to the diode under test. The capacitance at low temperatures (120 K) appears to be independent of voltage for moderately irradiated ($\Phi \sim 10^{14}$ n/cm^2) diodes [Fig. 1(a)]. This result indicates that the diode is fully depleted starting from the lowest dc reverse voltages when carrier generation centers (via an enhancement of the thermal emission lifetime) are suppressed by a temperature decrease, in diodes irradiated with $\Phi > 10^{13}$ n/cm^2.

The I-V characteristics at room temperature [Fig. 1(b)] measured by a Keithley-6430 electrometer show an increase of generation current with irradiation fluence within a reverse bias branch. At the same time, the forward current decreases with increasing fluence relative to its values in the less irradiated diodes. An increase of generation current implies a reduction of carrier recombination (capture) lifetime. This should result in the increase of recombination current at forward bias and the earlier saturation of the forward current. However, the observed decrease of the forward current in the heavily irradiated diodes hints to the reduction of the injection capability of the junction. Additionally, measurements of the I-V characteristics at low temperatures (<250 K) appear to be much more complicated, as the long relaxation to the steady current value makes these measurements unreliable. The I-V characteristics, measured at low temperatures, indeed depend on the rate of the voltage ramping (rate of measurement of each point on I-V), on the polarity and on the initial value of the applied voltage, and, therefore, these I-V characteristics are non–reproducible.

The analysis of LIV induced transients has been used to clarify the ambiguities caused by the competing barrier capacitance and generation ac currents within the C-V characteristics and of their phase shifts due to carrier capture-emission within boundary of depletion. The carrier generation/capture currents can exceed the depletion width modulation currents in heavily compensated material, especially when the ac voltage U_{ac} ramp becomes larger than the thermal potential, i.e., $U_{ac} > k_BT/e$. The increased generation currents lead to the misinterpretation of capacitance measurement, within simple C-V characteristics.

The technique of Barrier Evaluation by combined analysis of both reverse and forward polarity LIV pulsed current transients (BELIV) is proposed. The principles of the BELIV technique have been presented in Ref. 9, and details will be published elsewhere. Therefore, only a few aspects of the BELIV technique are mentioned briefly in view of its application in the present study.

The current transients are measured using a 50 Ω external resistor or load input of an Agilent Technologies DSO6012 A oscilloscope. Additionally, the measurement circuitry contains the adjustable output of a generator of linearly increasing voltage (GLIV) and the diode under investigation, connected in series. The other channel of the digital oscilloscope is used for synchronous control of linearity of the GLIV signal using a LIV pulse differentiating procedure installed within the DSO oscilloscope.

The simulated transients of the BELIV current components and of the total current are sketched in Fig. 2 for reverse (a) and forward (b) polarity LIV pulses, respectively.

The transient of the total reverse current (if the small diffusion component is ignored) at reverse polarity of LIV pulse is described by the sum of the barrier charging (i_C) and of the generation (i_{g-SC}) components as

$$i_{R\Sigma}(t) = i_C(t) + i_{g-sc}(t) = AC_{b0}\frac{1+\frac{U_C(t)}{2U_{bi}}}{\left(1+\frac{U_C(t)}{U_{bi}}\right)^{3/2}} + \frac{en_iSw_0}{\tau_g}\left(1+\frac{U_C(t)}{U_{bi}}\right)^{1/2}. \quad (1)$$

Here, $A = dU(t)/dt \cong U_P/\tau_{PL}$ is the ramp of the LIV pulse with a peak voltage U_P and a duration τ_{PL}. $C_{b0} = C(t=0)$ is the barrier capacitance determined by the built-in barrier U_{bi}. w_0 is the depletion width in the diode of junction area S, τ_g is the carrier generation lifetime within the space-charge region, n_i is the intrinsic carrier density, and $U_C(t) \cong At$ is the voltage drop over the diode, which increases linearly with time (t). Similarly, the components of barrier charging, of storage (diffusion) capacitance $i_{Cdif}(t) = (i_{dif0}/A)[(eU_F(t)/k_BT+1)exp(eU_F(t)/k_BT)-1]$ and of recombination current comprise the total current transients for the forward polarity LIV pulses. The simulated transients of the total current (Fig. 2(a) – reverse bias, and Fig. 2(b) - forward bias) excellently reproduce the main features of the experimental BELIV transients obtained for reverse [Fig. 3(a)] and forward [Fig. 3(c)] biasing, respectively.

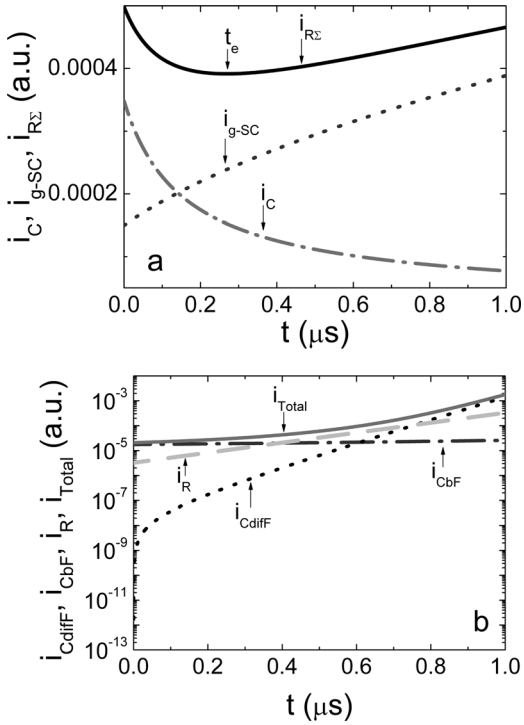

FIG. 2. Simulated transients, for a reverse (a) and forward (b) biased LIV pulse. The barrier charging/carrier extraction (i_C-dash-dot curve) component, the space-charge generation component (i_{g-SC} −dot), and the total current ($i_{R\Sigma}$-solid) composed of these components are shown in (a). The instant (t_e) for total current minimum is denoted in (a), as well. The simulated transients for a forward biased LIV pulse components (b) of the barrier charging (i_{CbF}- dash-dot curve), of the storage capacitance (i_{CdiffF} -dot), of the recombination current (i_R -dash) component, and the total current (i_{Total} -solid) composed of these components.

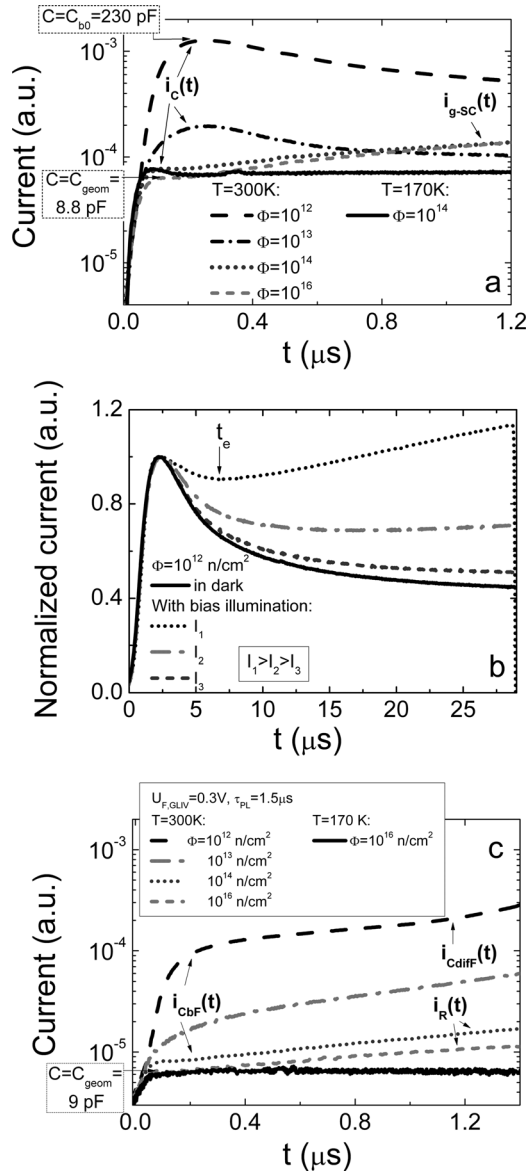

FIG. 3. Fluence dependent variations of experimental transients measured for reverse biased BELIV pulses without (a) and with (b) additional illumination as well as for forward biased (c) BELIV pulses. Here, the dominant components of current are indicated, respectively to those simulated in Fig. 2. In (a) and (c), the BELIV transients measured at room temperature are compared with those obtained at T = 170 K. Variations of reverse biased BELIV transients dependent on intensity of additional infrared illumination are illustrated in (b).

There is a possibility within the BELIV technique to extract the barrier capacitance at rather low applied voltages for each type of polarity LIV pulses. The charge extraction and generation current components can be determined from the fluence dependent experimental BELIV transients for reverse LIV pulses [Fig. 3(a)]. The reverse biased BELIV transient contains an initial peak ascribed to the equilibrium barrier capacitance C_{b0}, followed by a descending component of the charge extraction capacitance and an increasing component attributed to the generation current. Such a set of components of the reverse biased BELIV transient implies the existence of a current minimum [indicated by t_e in Figs. 2(a) and 3(b)] within the transient, which can be highlighted by varying the LIV pulse duration and/or the use of additional steady-state illumination [broken curves in Fig. 3(b)]. The generation current component becomes dominant for higher voltages ($U_r \geq 0.7$ V, corresponding to $t > 200$ ns for a single transient) within transients measured on reverse LIV pulsed diodes irradiated with $\Phi > 10^{13}$ n/cm^2 as illustrated in Fig. 3(a). The fluence range for the dominance of the generation current is in excellent agreement with that obtained when a clear separation between C_p and C_s characteristics appears in the C-V characteristics [Fig. 1(a)]. Thus, the evolution of the BELIV transients in Fig. 3(a) shows a monotonic increase of the generation current with increasing Φ. The nearly linear increase of generation current with fluence is also corroborated by the reverse bias I-V characteristics as shown in Fig. 1(b). The range of the dominance of generation current in BELIV and I-V characteristics corresponds well to the region of the "inversion sign" of effective doping.[1,3,4] The dominance of the generation current hides/disturbs the current phase shift measurements (the increased current due to generation of carriers in the space charge region leads to the seeming phase shift) by the LRC technique, due to which erroneous values of V_{FD} and N_{eff} are extracted. The dominance of generation current within BELIV transients indicates fast capture of carriers by high density of radiation induced traps (before emission). The decrease of the effective density of free carriers, caused by fast carrier capture, leads to an increase of a serial resistance

(in the electrically neutral material) and to the reduction of the current for the forward voltage branch. Fast carrier capture is also a reason for the decrease of the injection capability of junction and for the saturation of the forward current observed in heavily irradiated diode.

The barrier and storage capacitance currents dominate within forward biased BELIV transients [Fig. 3(c)], in the diodes irradiated with the smallest fluences of $\Phi < 10^{13}$ n/cm^2. The barrier capacitance, revealed by the initial amplitude of both the reverse and forward biased diode BELIV transients [Figs. 3(a) and 3(c)], decreases (in agreement with C-V's data in Fig. 1(a) for the fluence range $\Phi \leq 10^{13}$ n/cm^2) with increasing fluence. The model of the BELIV transients for a forward bias LIV predicts a built-in barrier shrinkage determined by the initial current (with zero storage capacitance for $t \approx 0$). For perfect diodes, the storage capacitance dominates in the ulterior stages of the BELIV transient. This is in agreement with measurements on the lowest fluence $\Phi \sim 10^{12}$ n/cm^2 irradiated diodes. For the storage capacitance induced current component (within backward stage of BELIV transient), a fast current increase with time is inherent. Only the very initial stage of this component is noticeable in Fig. 3(c), as a feasibly small U_P has been intentionally selected in order to be able to observe both the depletion and storage capacitance attributed components. However, this storage capacitance component decreases with increasing fluence and it fully disappears for $\Phi > 10^{13}$ n/cm^2. It is outrivaled by the recombination current component, which shows a nearly linear increase with LIV voltage (for $\Phi > 10^{13}$ n/cm^2). This result shows, that even for the moderately irradiated diodes, the forward voltage does not govern the junction and carrier injection. This can happen, if the diode is completely depleted at equilibrium. Then the diode behaves like a capacitor, this is illustrated in Fig. 3(c) where the initial BELIV step represents the geometrical capacitance for $\Phi > 10^{13}$ n/cm^2.

Thus, the observed fluence dependent variations [Fig. 3(c)] of the forward biased BELIV transients, for $\Phi > 10^{13}$ n/cm^2, are in agreement with changes in the I-V characteristics for the forward voltage (FV) branch [Fig. 1(b)]: the decrease of the forward current relative to its values in the less irradiated diodes and the possibility to apply a relatively large forward voltage on heavily irradiated diodes indicate the full depletion regime. Built-in full depletion can be reached when radiation defects compensate completely the dopants. In that case nearly all "native" doping induced free carriers are captured by the large density of radiation induced traps, while only a small fraction of these traps are filled due to a lack of free carriers. The routine interpretation of C-V measurements is incorrect in such a situation, as the ac voltage only mediates the recombination–generation current variations, especially if $U_{ac} > k_B T/e$. The dielectric relaxation time for fully compensated material becomes very long.

The total BELIV current for the above described full depletion voltages can be calculated (similarly to the method used in Ref. 11) by considering the conductivity and displacement current components over the sample thickness d for variable voltage and surface charge changes on electrodes using standard boundary conditions (for electric field $E|_{x=d} = 0$, $dE/dx|_{x=d} = 0$ and potential $V|_{x=d} = 0$). This solution is expressed as

$$i(t)_{FD} = eS\frac{d}{2}\left(\frac{dn}{dt} + \frac{dp}{dt}\right) + \frac{\varepsilon\varepsilon_0 S}{d}\frac{dU_C}{dt}. \quad (2)$$

This solution (for over-depleted diode and nearly equal carrier transit τ_{tr} and thermal emission τ_{em} lifetimes, $\tau_{tr} \sim \tau_{em}$, as well as using relations $|dn/dt| = n_0/\tau_{em} \approx n_0/\tau_{tr}$, $n \approx n_0 = N_D$), can be approximated as

$$\begin{aligned} i(t)_{FD} &\approx eS\frac{d}{2}\frac{n_0}{\tau_{tr}} + C_{geom}\frac{dU_C}{dt} \\ &= e\frac{S}{2d}n_0\mu_n U_C(t) + C_{geom}\frac{dU_C(t)}{dt}. \end{aligned} \quad (3)$$

Hereby, it is assumed that the geometrical capacitance C_{geom} is given by $C_{geom} = \varepsilon_0\varepsilon S/d$, μ_n is mobility of electrons, $\tau_{em} = 1/\sigma_c v_T N_C \exp(-E_{TC}/k_B T)$, $\tau_{tr} \cong d^2/\mu_n U$. It is clear that for insulating material, the BELIV transient takes the shape typical for a pure capacitor with a current value of $i_{CFD} = C_{geom}(dU_C/dt)$ [solid curves in Figs. 3(a) and 3(c)]. The voltage drop on load resistor (being a solution of current equation for RC circuit with LIV pulse) represents the square-wave pulse if C is constant. For compensated material full of traps, a further increase of the voltage above U_{FD} shows the current enhancement transient $i_{emFD}(t) = e(S/2d)n_0\mu_n U_C(t)$, which is added to i_{CFD}.

A similar situation appears in C-V characteristics for harmonic ac voltages of frequency f, capable of ensuring the necessarily short carrier transit time $\tau_{tr} \cong d^2/\mu_n U < t_{em} \cong f^{-1}$. The emission time τ_{em} for trapped (n_T) carriers depends on the capture cross-section σ_c and thermal velocity v_T and on the effective density of band states N_C as well as on the thermal activation energy E_{TC} of the trap. Then, if the dc voltage is sufficient to collect all the trapped charge (of value close to equilibrium density n_0 of "native" carriers) within built-in fully depleted material, the measured C-V response saturates. This voltage seems to be wrongly ascribed to a full depletion state and to the space charge sign inversion effect in Refs. 1–5, and 7.

III. DISCUSSION

The above discussion has been made using terminology common in semiconductor device physics. Actually, the high resistivity material, irradiated with fluences $\Phi \gg 10^{13}$ n/cm^2, becomes an insulator. Then, common concepts used for the analysis of device and of junction operation such as a depletion width and effective doping should be applied with care. If heavily irradiated diodes, which are not isolated well from the external factors, such as background light, the Debye screening length can be modified by several orders of magnitude.[12] In a more general approach, the initial high resistivity material, which contains a rather small density of "native" free carriers to sustain conduction, experiences a transition to a dielectric state, characterized by $RC = (d/Se\mu_{eff}n_{eff}) \times (\varepsilon\varepsilon_0 S/d) = \varepsilon\varepsilon_0/e\mu_{eff}n_{eff}$, with $n_{eff} \cong n_0$ and $\mu_{eff} \cong \mu_n$, for high fluences of irradiation. The effective density of free carriers n_0, that will react to an external test

voltage and that can sustain a depletion boundary, decreases (approaching to zero) when the carrier capture times become significantly shorter than the inter-band thermal generation time. Then, n_{eff} is considerably smaller than the intrinsic density n_i, i.e., $n_{eff} \ll n_i$, and it does no longer make sense to speak about majority/minority carriers and junction effects.

For n-type material (as the diode base) with initial donor density N_D, the radiation traps (of density $N_{T\pm}$) with levels in the upper half of the forbidden band-gap are responsible for the time-dependent processes, while acceptors (N_{A-}) below the midgap can serve as compensating centers $N_{Deff} = (N_D - N_{A-})$, as discussed in Ref. 11. The heavily irradiated diodes usually contain both types of traps ($N_{T\pm}$ and N_{A-}). Therefore, it is helpful to consider briefly the characteristic times and depths, as introduced by radiation defects and other external factors. These simulated dependencies are illustrated in Fig. 4.

The capacitance techniques based on charge extraction (for incomplete diode depletion) are applicable provided that the dielectric relaxation time $\tau_M = \varepsilon\varepsilon_0/e\mu n_0$ is the shortest one for the non-equilibrium system. During this τ_M time, the diffusion-drift processes are steady at the depletion boundary, and the depletion width w is defined with the precision of the Debye length L_D. Thus initial delays in the range of $t < 10^{-7}$ s of the BELIV pulse can be significant in high resistivity or compensated materials [Figs. 3(a), 3(c), and 4(a)]. With increasing of the external voltage U_C over the diode, the depletion width w approaches to the geometrical diode thickness d. Therefore, the carrier transit time decreases to its value $\tau_{tr} \cong d^2/\mu U_C|_{FD}$ at geometrical capacitance (FD = full depletion). After the diode is completely depleted, τ_{tr} may become shorter than τ_M with further voltage increase [Fig. 4(a)]. In that case, carriers flow across the inter-electrode gap. For $\tau_M \geq t_{tr}$ the material should behave as an insulator, and any carrier generated within the inter-electrode space should disappear during $\tau_{tr} = \tau_{TOF}$ given by the time of flight (TOF). Some of these characteristic times depend on the effective doping ($N_{Deff} = N_D - N_A$) of the material, and therefore also on the density of compensating traps (N_A). However, only a small fraction of these possible compensating centers is occupied, if $N_A \gg N_D = n_0$. In reality, only the equilibrium "native" carriers caused by shallow dopants are redistributed among the deep traps when the deep traps density approaches to or exceeds the dopant density in order to reach the charge neutrality in equilibrium. The maximal density n_0 of these redistributed carriers is equal to the initial doping density N_D. Neutron transmutation effects can be ignored, as irradiation with reactor neutrons with 1 MeV equivalent energy are studied. The irradiated diode may thus become a capacitor with a completely depleted base even without external bias and this case can easily be identified by a square-wave BELIV pulse shape, observed for instance in Figs. 3(a) and 3(c). It can be noticed in Fig. 4(a), that the FD regime for $d = 300$ μm and $N_{Deff} = 1.5 \times 10^{11}$ cm^{-3} is reached at $U_r \sim 10$ V. Consequently, the simple C-V measurements make sense only for $U_r < 20$ V and for a frequency range of $f \ll 1/\tau_M$. A further decrease of N_{Deff} leads to an enhancement of the dielectric relaxation time and to the reduction of the range for applied f and U_r. Therefore, it is necessary to consider characteristic times together with inherent depths for fluence dependent changes of density of the rather deep traps.

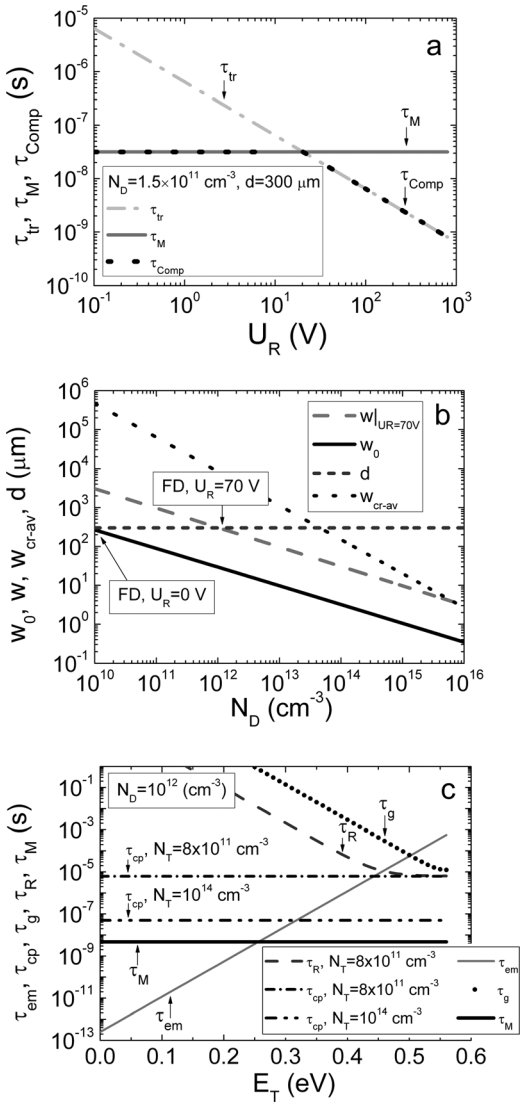

FIG. 4. (a) Comparison of the dielectric relaxation (τ_M -solid), transit (τ_{tr} -dot-dash), and composite (τ_{Comp} -large dots) times as a function of applied reverse voltage for a diode of 1.5×10^{11} cm^{-3} effective doping density and of geometrical thickness d = 300 μm. (b) Simulated characteristic lengths of equilibrium barrier width (w_0 -solid line), of depletion width (w -dash) at $U_R = 70$ V and of a critical width ($w_{cr\text{-}av}$ -dots) for avalanche breakdown due to impact ionization as a function of effective doping density for a 300 μm thick diode (shown as horizontal curve). (c) Carrier emission (τ_{em}), capture (τ_{cp}), generation (τ_g), and recombination lifetime (τ_R) as a function of deep level position E_T in the upper half of the forbidden-gap in n-type ($N_D = 10^{12}$ cm^{-3}) material compared with dielectric relaxation time (τ_M). Capture lifetimes are shown for trap density $N_T = 8 \times 10^{11}$ cm$^{-3} < N_D$ and for $N_T = 10^{14}$ cm$^{-3} \gg N_D$.

Characteristic lengths simulated for diodes of $d = 300$ μm thickness as a function of effective doping are illustrated in Fig. 4(b). It can be observed, that for significantly compensated material (with N_{eff} close to the intrinsic $n_i \sim 10^{10}$ cm^{-3} at room temperature) the diode is completely depleted without bias. Thus, the depletion width can be bias dependent only in the range of voltages $U_r < 70$ V starting from the full depletion voltage $U_{FD} \cong 70$ V for non-irradiated

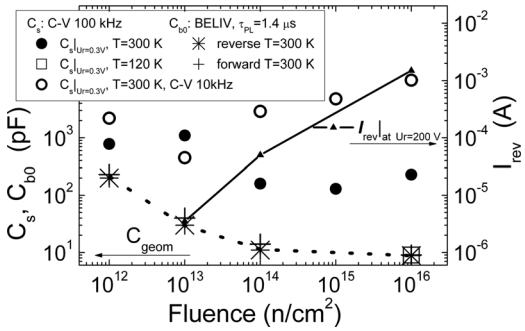

FIG. 5. Comparison of the fluence dependent variation of serial capacitance C_s (circles) at reverse voltage of about 0.3 V measured using 10 kHz (open circles) as well as 100 kHz (solid circles) at 300 K and 120 K (open squares) temperatures, of the barrier capacitance C_{b0} measured by BELIV technique using both reverse (stars) and forward (crosses) LIV pulses (left scale) at T = 300 K, and of reverse current (right scale) extracted from I-V characteristics at 200 V reverse voltage.

material ($N_D \sim 10^{12}$ cm^{-3}). The widely used model of the space charge sign inversion[1–4] to analyze characteristics of heavily irradiated Si thick detectors (using $N_{eff} \geq 10^{14}$ cm^{-3}) seems not to be applicable, as avalanche breakdown caused by impact ionization should appear for critical depletion lengths $w_{cr} > 150$ μm at $N_{eff} \geq 10^{14}$ cm^{-3}, as illustrated in Fig. 4(b). This dependence has been simulated using critical depth as $w_{cr\ av} = 2.67 \times 10^{10} \times N_A^{-7/8}$ for impact ionization in a parallel plate junction.[8] Similar values of w_{cr} can be obtained using an alternative approach ($w_{cr\ av} = 2 \times 10^{11} N_D^{-1}$).[11] Thus, full depletion cannot be reached for moderately doped $N_{Deff} \sim 10^{14}$ cm^{-3} thick diodes. The possibility to apply rather high reverse voltages ($\gg 70$ V) to heavily irradiated diodes,[1] without any avalanche effects, clearly indicates that built-in full depletion dominates (as opposed to sign inversion). Avalanche breakdown should change the composite time due to plasma processes, assuming that these processes are developed on the picasecond time scale. However, in our experiments on charge collection transients, avalanche processes were clearly identified when the excess carrier densities, generated by short laser pulses, approached to n_0 with $w_{cr} \cong 2.7 \times 10^{10} N_{eff}^{-7/8}$, $U_{r\ cr} \cong 5.3 \times 10^{13} N_{eff}^{-3/4}$ (Ref. 8) as shown in Fig. 4(b).

As a result, the capacitance based traditional techniques such as C-V and deep level transient spectroscopy (DLTS) are hardly applicable when characteristic transit times become shorter than the dielectric relaxation time τ_M, and characteristic lengths w_0, w_{cr-av} exceed the sample thickness. Actually, the additional currents generated in the diode dominate over the junction capacitance i_C current, and these (e.g., C-V) signals can be misinterpreted for heavily irradiated devices. The additional currents can be attributed to the characteristic times of carrier capture (τ_{cp}), emission (τ_{em}), generation (τ_g) for current within the space charge region, and to recombination lifetime (τ_R) for currents generated within diffusion/Debye lengths nearby the depletion boundary. The capture time $\tau_{cp} = 1/\sigma_c v_T (N_T - n_T(t))$ is determined by the capture cross-section σ_c, the thermal velocity v_T of carriers, and the density $(N_T - n_T(t))$ of empty traps N_T (at $n_T = 0$). The emission time for trapped (n_T) carriers $\tau_{em} = 1/\sigma_c v_T N_C \exp(-E_{TC}/k_B T)$ depends on the same σ_c, v_T and on the thermal activation energy E_{TC} of the trap. More rigorously, the coefficient γ of carrier localization/de-localization from traps obtained using distribution functions[13] should be used instead of the product $\sigma_c v_T$. The space charge region generation lifetime includes sequential emission of a hole and an electron by a trap and is expressed using Shockley-Read-Hall (S-R-H) statistics[2–5,8,9,11–13] as $\tau_g = 2\cosh(E_T - E_i)/\sigma_c v_T N_T$. Here, the position of the deep level E_T is specified relatively to the half-gap E_i level. The recombination lifetime in the free carrier (n_0) rich region is$\tau_R = [1 + 2(n_i/n_0)\cosh(E_T - E_i)]/\sigma_c v_T N_T \approx 1/\sigma_c v_T N_T$|ifni $\ll$ n0within the S-R-H model. Here, again the sequential capture of an electron and a hole is assumed, and Langevin type recombination[14,15] is ignored. Generally, the simple S-R-H model is only valid when the traps concentration is smaller than the free carrier density, and carrier recombination is characterized by the carrier pair lifetime. These simulated lifetimes as functions of the deep trap activation energy E_T and density N_T are sketched in Fig. 4(c). As usually, conditions for simple S-R-H statistics are not fulfilled for irradiated materials. Actually, the microscopic lifetimes such as τ_{cp}, τ_{em} should be used instead of the characteristic lifetimes associated with the S-R-H model, e.g., τ_g, when the density of traps of different species significantly exceeds the density of carriers (n_0).

It can be noticed in Fig. 4(c) that the shortest carrier lifetime is the one for emission τ_{em} ascribed to the shallow traps. Thus, the thermal emission process can be identified even in heavily compensated material when $\tau_{em} < \tau_M$. However, emission can be observable in macroscopic characteristics also provided τ_{em} approaches to τ_{cp}, as traps can be noticeably filled only if $\tau_{cp} < \tau_{em}$. This condition can be satisfied for Si with a large density of thermal donors (ensuring short τ_{cp} and τ_{em}), which are characterized by rather shallow levels ($\geq$0.1 eV) and are capable to rapidly follow the voltage changes and to partially restore the depletion boundary.

The carrier capture time τ_{cp} decreases with increasing density of traps. Then trap filling can be steady if emission time is rather long $\tau_{em} \sim \tau_{cp}$ for the definite species of traps (moderately shallow). The τ_{cp} values are short and constant, when only a small fraction of the deep traps is filled by captured carriers. The excess carrier recombination lifetime $\tau_R \sim \tau_{cp}$, measured on heavily ($\sim 10^{16}$n/cm^2) irradiated diodes by microwave probed photo-conductivity transients, show values of $\sim$200 ps.[16] The condition $\tau_{em} > \tau_{cp} > \tau_M$ is the basis of DLTS and C-V techniques based on the averaging of repeated measurements. The variety of processes, determined by different ratios of characteristics times, is rather wide,[11] especially when carrier redistribution among centers of several species takes place. The sequenced processes of generation (τ_g) and recombination (τ_R) are longer than the microscopic ones described by τ_{em} and τ_{cp}, if simple statistics for a single dominant level can be applied. The relations among the discussed lifetimes are essential in the analysis of the components in transients, when redistribution of electric field due to carriers generated within depletion region takes place, and filling of states is changed by different external factors, such as the application of bias light and primary injection changes the occupation of deep centers.

Variations of C_s extracted from C-V characteristics, of the reverse current for a 200 V biased diode measured by I-V characteristics, and of the initial barrier capacitance C_{b0} evaluated by both reverse and forward LIV pulses are generalized in Fig. 5. It is obvious, that the barrier capacitance estimated by the BELIV technique approaches to the geometrical C_{geom} for fluences $\Phi > 10^{13}$ n/cm^2. These C_{b0} values are significantly smaller than C_s extracted from the C-V characteristics at $U_{R,C-V} \sim 0.3$ V values comparable to the BELIV regime for $t < 200$ ns. This result can be understood by the elevated generation currents and the significantly increased dielectric relaxation time in the C-V characteristics. The C_s values measured by C-V at small reverse voltage (Fig. 5) do not show any clear dependence on fluence and the measured values considerably depend on test signal frequency, while experimental errors are rather large. The initial barrier capacitance C_{b0} evaluated by both reverse and forward BELIV pulses lies within the measurement errors that do not exceed the size of the symbols in Fig. 5 and are a clear indication of the decrease of absolute C_{b0}values due to the increase of depletion width.

IV. SUMMARY

In summary, the presented analysis by combining C-V, I-V, and BELIV techniques enabled to clarify the conditions of full depletion in heavily irradiated Si detectors. It has been shown that built-in full depletion (the insulating state) is inherent for 300 μm thick n-type Si diodes doped with 10^{12} cm^{-3} donors and irradiated with hadron fluences above 10^{13} cm^{-2}. In other words, high resistivity material irradiated with fluences $\Phi > 10^{13}$ n/cm^2 becomes an insulator, and common concepts used in the analysis of device and of junction operation such as depletion width, effective doping density should be used with care.

It has been shown that the barrier evaluation by the linearly increasing voltage (BELIV) method can be a useful extension of transient techniques for the separation of barrier charging and carrier capture/emission currents. The BELIV pulsed technique enables to clarify a few significant aspects: to identify the charge extraction regime and to estimate the barrier capacitance, to clarify the competition between barrier and storage capacitance and the generation/recombination currents, and to clarify the full depletion state for heavily irradiated diodes.

It has also been shown that radiation defects induced sign inversion effects and fatally elevated voltages of full depletion are artifacts due to the application of standard C-V measurements in the complicated case of transition from semiconductor to insulator, when carrier emission and capture currents approach values of the barrier charging currents. Also, I-V current non-stabilities at cryogenic temperatures have been found in irradiated diodes, starting from moderate fluences. These non-stabilities are caused by the significant increase of the dielectric relaxation time when carriers are captured to deep centers. Values of current in I-V's are non-stabilized, when the dielectric relaxation time is longer than a time-gap between the adjacent measurements on the dc I-V characteristic. This additionally proves the existence of the built-in full depletion (insulating) state in heavily irradiated diodes.

ACKNOWLEDGMENTS

G. Kramberger is acknowledged for the neutron irradiations at the TRIGA reactor. K. Smith and J. Vanhellemont are appreciated for help in editing the manuscript and valuable suggestions. This work was supported by the Lithuanian Science Council Grant MIP-11018.

[1]See www.cern.ch/rd50 for more information on RD Status Report 2002/2003.
[2]M. Huhtinen, Nucl. Instrum. Meth. Phys. Res. A **491**, 194 (2002).
[3]G. Lutz, *Semiconductor Radiation Detectors* (Springer, Heidelberg, 2007).
[4]H. Spieler, *Semiconductor Detector Systems* (Oxford University Press, New York, 2005).
[5]V. Eremin, N. Strokan, E. Verbitskaya, and Z. Li, Nucl. Instrum. Meth. Phys. Res. **A 372**, 388 (1996).
[6]Z. Li, Nucl. Instrum. Meth. Phys. Res. **A 360**, 445 (1995).
[7]D. Campbell, A. Chilingarov, and T. Sloan, Nucl. Instrum. Meth. Phys. Res. **A 492**, 402 (2002).
[8]B. Y. Baliga, *Power Semiconductor Devices* (PWS, Boston, 1995).
[9]E. Gaubas, T. Čeponis, J. Kusakovskij, A. Uleckas, S. Sakalauskas, and J. Vaitkus, "Evaluation of fluence dependent variations of capacitance and generation current parameters by transient technique," presented at RD50 Workshop, Barcelona (2010), www.cern.ch/rd50.
[10]G. Juška, K. Arlauskas, M. Viliunas, and J. Kocka, Phys. Rev. Lett. **84**, 4946 (2000).
[11]P. Blood and J. W. Orton, *The Electrical Characterization of Semiconductors: Majority Carriers and Electron States* (Academic, London, 1992).
[12]S. M. Ryvkin, *Photoelectric Effects in Semiconductors* (Consultants Bureau, New York, 1964).
[13]J. S. Blakemore, *Semiconductor Statistics* (Pergamon, New York, 1962).
[14]A. Pivrikas, G. Juška, R. Österbacka, M. Westerling, M. Viliunas, K. Arlauskas, and H. Stubb, Phys. Rev. B **71**, 125205 (2005).
[15]M. Pope and C. E. Swenberg, *Electronic Processes in Organic Crystals and Polymers* (Oxford University Press, New York, 1999).
[16]E. Gaubas, A. Uleckas, and J. Vaitkus, Nucl. Instrum. Meth. Phys. Res. **A 607**, 92 (2009).